

Application of a semi-Lagrangian scheme in the relativistic regime of laser interaction with an overdense plasma slab

D. Del Sarto ^{*}, A. Ghizzo, T. Réveillé, N. Besse, P. Bertrand

Laboratoire de Physique des Milieux Ionisés et Applications, CNRS UMR 7040, BP 239 54506, Vandoeuvre-les-Nancy cedex, France

Available online 25 May 2007

Abstract

A one-dimensional relativistic semi-Lagrangian Vlasov–Maxwell code is here outlined in an application to the simulation of the interaction of relativistically strong laser pulses with overdense plasmas. Algorithmic differences are briefly recalled with respect to the regimes for which a straightforward time-splitting scheme is applicable. As an example of the accuracy of the semi-Lagrangian scheme, we present some strictly kinetic features of the penetration process of an intense laser pulse inside an overdense plasma by self-induced transparency. In particular we show the formation of vortical trapping structures in the electron distribution function, due to the beat-wave process between the incident laser light and the doppler-shifted reflected wave. These coherent structures are later destroyed due to the formation of an electron-cavitation, which develops close to the density peak near the propagating front-wave, thus separating the relativistically underdense and overdense regions.

© 2007 Elsevier B.V. All rights reserved.

PACS: 02.60.Cb; 02.60.Jh; 52.38.Dx; 52.38.Kd; 52.65.Fh

Keywords: Vlasov plasma; Semi-Lagrangian; Self-induced transparency; Electron cavitation

1. Introduction

Experimental investigation of laser–plasma interactions in relativistic regimes is nowadays possible, since intensities above 10^{19} W cm⁻² are now achievable to short laser pulses. In particular, relativistic effects (i.e. the relativistic increase of electron inertia) allow laser propagation through an overdense plasma up to length scales for which the propagation would be classically forbidden. In overdense plasmas, in which the density n is greater than the critical value $n_c \approx 1.1 \times 10^{21} \lambda_0^2$ cm⁻³ (where λ_0 is the laser wavelength expressed in microns), the incident electromagnetic radiation is damped over a distance of the order of the electron skin-depth, $d_e = c/\omega_{pe}$, with $\omega_{pe}^2 = ne^2/m_e\epsilon_0$. In the high laser intensity regime, the quiver velocity of electrons becomes relativistic and the resulting increase of electron inertia (i.e. $m_e \rightarrow \gamma m_e$, with γ the relativistic Lorentz factor)

^{*} Corresponding author.

E-mail address: del.sarto@impi.uhp-nancy.fr (D. Del Sarto).

decreases the effective plasma frequency thus modifying the optical properties of the plasma. In particular, the effective damping scale of the incident light is increased ($d_e^2 \sim \gamma m_e$) and intense laser pulses can propagate through overdense plasmas; this is known as self-induced-transparency (SIT) effect. We do not consider here other relativistic effects such as laser self-focusing because of the geometry approximation we will next restrict to. Laser plasma interactions in relativistic regimes thus provide new features for electromagnetic waves' propagation, which assumes a strongly non-linear character. The modelling and comprehension of these effects are of fundamental interest for technical applications such as the fast ignition fusion concept [1], photon or ion accelerators, and X-ray lasers.

In this paper, we discuss a semi-Lagrangian Vlasov scheme, one-dimensional in space (1D) and in velocity (1V), and we show its first application to the propagation, due to SIT effects, of a circularly polarized light inside an overdense plasma. Although PIC codes represents an efficient method to investigate laser–plasma interaction, the corresponding simulation results are of somewhat difficult interpretation, since PIC models tend to suffer from poor statistical resolution of particles motion, due to numerical noise and limitations in the number of particles. Semi-Lagrangian schemes provide an opportunity to adequately describe non-linear particle dynamics in detail, even in the strong relativistic regimes such as in SIT. The paper is structured as it follows. In Section 2 we outline the architecture of the integration algorithm and we point out the differences with respect to a time-splitting model applicable to non-relativistic regimes. In Section 3 the algorithm procedure is explicated for the equations of the sample-system we consider here, and in Section 4 the initial conditions and the numerical results are given. A concluding summary follows in Section 5.

2. Semi-Lagrangian integration scheme

The semi-Lagrangian integration scheme has been extensively discussed in Refs. [2,3]. It provides an efficient computational algorithm to solve the Vlasov–Maxwell system equations even if the divergence of the velocity field in phase-space is not separable between spatial and momentum coordinates. Let us consider Vlasov equation written in the conservative form:

$$\frac{\partial f_\alpha}{\partial t} + \mathbf{V}_{\mathbf{X}_\alpha} \cdot [\mathbf{U}_\alpha(\mathbf{X}_\alpha, t)f_\alpha] = 0 \quad (1)$$

where $\mathbf{X}_\alpha = (\mathbf{q}_\alpha, \mathbf{p}_\alpha)$ is the vector of phase-space coordinates for the specie α , and $\mathbf{U}_\alpha = \dot{\mathbf{X}}_\alpha$ is the corresponding velocity-field, which is divergence-free thanks to Liouville's theorem; the gradient vector is $\mathbf{V}_{\mathbf{X}_\alpha} = (\partial/\partial \mathbf{q}_\alpha, \partial/\partial \mathbf{p}_\alpha)$. Explicitly stating the dependence on canonical variable in the most general case, we rewrite Eq. (1) as:

$$\frac{\partial f_\alpha}{\partial t} + \mathbf{V}_{\mathbf{q}_\alpha} \cdot [\dot{\mathbf{q}}_\alpha(\mathbf{q}_\alpha, \mathbf{p}_\alpha, t)f_\alpha] + \mathbf{V}_{\mathbf{p}_\alpha} \cdot [\dot{\mathbf{p}}_\alpha(\mathbf{q}_\alpha, \mathbf{p}_\alpha, t)f_\alpha] = 0 \quad (2)$$

The solution of Eq. (2) is equivalent to the solution of two separate advection equations with respect to the \mathbf{q} and \mathbf{p} coordinate in the phase space, but in the “most general” (mathematically speaking) case, two source terms would provide the coupling between the canonical variables advecting each equation (r.h.s. terms in the following equation):

$$\frac{\partial f_\alpha}{\partial t} + \dot{\mathbf{q}}_\alpha \cdot \frac{\partial f_\alpha}{\partial \mathbf{q}_\alpha} = -f_\alpha \frac{\partial \dot{\mathbf{q}}_\alpha}{\partial \mathbf{q}_\alpha}, \quad \frac{\partial f_\alpha}{\partial t} + \dot{\mathbf{p}}_\alpha \cdot \frac{\partial f_\alpha}{\partial \mathbf{p}_\alpha} = -f_\alpha \frac{\partial \dot{\mathbf{p}}_\alpha}{\partial \mathbf{p}_\alpha} \quad (3)$$

It is worth remarking however that whenever particle spatial velocity $\dot{\mathbf{q}}_\alpha$ is not depending on position \mathbf{q} itself, the two source terms are zero ($\partial \dot{\mathbf{q}}_\alpha / \partial \mathbf{q}_\alpha = 0$ implying $\partial \dot{\mathbf{p}}_\alpha / \partial \mathbf{p}_\alpha = 0$ because of Liouville's theorem), as it occurs in most non-relativistic and relativistic regimes, when spatial and velocity variables have the same dimensionality. In these cases a straightforward Eulerian time-splitting method can be performed, in which the space- and the speed-divergence terms are separately advanced in time (Ref. [4]) with respect to the initial coordinate grid. Nevertheless, while in non-relativistic regimes such as those discussed in Ref. [7] the Eulerian time-splitting is usually always applicable, a most interesting case with $\partial \dot{\mathbf{q}}_\alpha / \partial \mathbf{q}_\alpha \neq 0$ is provided by relativistic, spatially inhomogeneous Vlasov systems in which some exact invariants exist, e.g. in relativistic 1D + 2V, 1D + 3V, or 2D + 3V problems. In these configurations the translational invariance along some spatial coordinate implies

the conservation of the related conjugated momentum, which so becomes a constant, generally depending on space through fields' spatial dependence; this dependence enters in $\dot{\mathbf{q}}_\alpha$ through the relativistic γ -factor (e.g. in cartesian coordinates: $\dot{\mathbf{q}}_\alpha = \mathbf{p}_\alpha / (m_\alpha \gamma_\alpha)$), which becomes $\gamma_\alpha = \gamma_\alpha(\mathbf{q}_\alpha, \mathbf{p}_\alpha)$. Due to this, the presence of r.h.s. terms in Eq. (3) invalidates the time-splitting approach by making the two l.h.s. advection equations of Eq. (3) not separately solvable. As shown in Ref. [3], indeed, the application of the traditional time-splitting method to the non-separable case would lead to cumulative numerical error at each time step, which would waste the density conservation beyond the accuracy needed for the consistency of the scheme. This because the source terms in Eq. (3) would not be solved at equal times, and therefore they would not cancel out as it is mathematically required by Liouville's condition.

An alternative computational method applicable to this non-separable case is provided by the backward semi-Lagrangian scheme [2], which uses a direct multi-dimensional advection. The semi-Lagrangian scheme computes the value of the function f at time $t_n + \Delta t$, by shifting it in time from t_n along the Lagrangian characteristics of the system. Notice that the position in the phase-space, of f at time t_n along a characteristic, is in general not corresponding to a mesh-point. This scheme is however called just "semi"-Lagrangian because it uses in fact an Eulerian grid, and the value of f_α at the point on the characteristic at time $t_n + \Delta t$ is computed by interpolation from the value which f_α assumes at the mesh-points at t_n . We now briefly recall the algorithm outline, by remanding to the master references (Refs. [2,3]) for further details.

By defining the characteristics of Eq. (1) as $d\mathbf{X}/dt = \mathbf{U}(\mathbf{X}(t), t)$, from the advective form of Eq. (1) it is found that f is constant along the characteristics:

$$f[\mathbf{x}, t_n + \Delta t] = f[\mathbf{X}(t_n; \mathbf{x}, t_n + \Delta t), t_n] \quad (4)$$

With the notation $\mathbf{X}(t; \mathbf{x}, s)$ we indicate the solution of the characteristics equation whose value is \mathbf{x} at time s ; in Eq. (4) we have taken $s = t_n + \Delta t$. The advection algorithm consists of two steps. First, we find the starting point (at time t_n) of the characteristic ending in \mathbf{x} (at time $t_n + \Delta t$). The characteristic equation is solved by finite-difference approximation with a two time-step scheme (so to maintain second order accuracy) since no explicit analytic expression is *a priori* given about \mathbf{U} . The resulting relation,

$$\mathbf{X}(t_n) = \mathbf{x} - \Delta t \mathbf{U}(\mathbf{X}(t_n + \Delta t/2), t_n + \Delta t/2) \quad (5)$$

leads to an iterative expression for an appropriate vector \mathbf{d} in phase-space, which is defined so to satisfy $\mathbf{X}(t_n + \Delta t/2) = \mathbf{x} - \mathbf{d}$. By using the relation $\mathbf{X}(t_n + \Delta t/2) = [\mathbf{X}(t_n + \Delta t) + \mathbf{X}(t_n)]/2$, which is still valid to the second order, it is found $\mathbf{X}(t_n) = \mathbf{x} - 2\mathbf{d}$ and thus $\mathbf{d} = (\Delta t/2)\mathbf{U}(\mathbf{x} - \mathbf{d}, t_n + \Delta t/2)$. This latter expression is solved iteratively to evaluate \mathbf{d} . The second step of the Lagrangian scheme consists in the computation of $f[\mathbf{X}(t_n; \mathbf{x}, t_n + \Delta t), t_n] = f[\mathbf{x} - 2\mathbf{d}, t_n]$ by interpolating with cubic B-splines the value of f in the mesh-points at time t_n . Cubic spline-interpolation represents a good compromise; linear interpolation for f would be too dissipative, whereas it is sufficient for \mathbf{U} while using cubic splines for f (see e.g. Refs. [2,5]). The values of f at the $t_n + \Delta t$ time are then found by using Eq. (4).

3. Application to an interaction between a circularly polarized laser and a plasma in one-dimensional geometry

We consider an application to the semi-Lagrangian 1D–1V integration scheme to the 1D–3V model for a laser–plasma interaction in the case of circularly polarized light (see Ref. [3]). This technique of direct 2D-advection (i.e. without time-splitting) is required for the study of laser plasma interaction in the relativistic regime in which SIT occurs. By assuming 1D spatial geometry (i.e. dependence on the x variable only), the orthogonal components of particles' canonical momentum $\Pi_\alpha = \mathbf{p}_\alpha + q_\alpha \mathbf{A}$ is conserved ($d(\Pi_{\alpha,\perp})/dt = \nabla_{\mathbf{q}_{\alpha,\perp}} \mathcal{H}_\alpha = 0$) so that explicit dependence on p_x only can be considered and a 1D–1V integration scheme can be used. Here and thereafter \mathbf{A} is the usual electromagnetic potential vector, and $\mathcal{H}_\alpha = m_\alpha c^2 (\gamma_\alpha - 1) + q_\alpha \phi(x, t)$ is the Hamiltonian of an α -specie particle. By assuming for simplicity and no loss of generality the case of a plasma prepared so that $\Pi_\alpha = 0$, with one-time ionized atoms (i.e. $q_i = e$), Lorentz' factor is written as $\gamma_\alpha = \sqrt{1 + p_{x,\alpha}^2 / (m_\alpha c)^2 + e^2 \mathbf{A}_\perp^2(x, t) / (m_\alpha c)^2}$. The corresponding Vlasov equation is

$$\frac{\partial f_\alpha}{\partial t} + \frac{p_{x,\alpha}}{m_\alpha \gamma_\alpha} \frac{\partial f_\alpha}{\partial x} + \left(q_\alpha E_x - \frac{e^2 m_\alpha c^2}{2\gamma_\alpha} \frac{\partial \mathbf{A}_\perp^2}{\partial x} \right) \frac{\partial f_\alpha}{\partial p_{x,\alpha}} = 0 \quad (6)$$

With the notation introduced in Section 2 (Eq. (1)) we have $\mathbf{X}_\alpha = (x, p_{x,\alpha})$ and

$$\mathbf{U}_\alpha = \left(\frac{p_{x,\alpha}}{m_\alpha \gamma_\alpha}, q_\alpha E_x - \frac{e^2 m_\alpha c^2}{2\gamma_\alpha} \frac{\partial \mathbf{A}_\perp^2}{\partial x} \right) \quad (7)$$

However, in order to perform the time-shift along the characteristic it is necessary to evaluate \mathbf{U}_α (see Eq. (5)), and thus the electromagnetic fields E_x and \mathbf{A}_\perp , at the time $t_n + \Delta t/2$. This task is accomplished by solving also Maxwell equations along the characteristics, following the standard approach as described e.g. in Ref. [3]. We remand to the reference for some explicit example; here we just recall the definitions

$$n_e = \int f dp_{x,e}, \quad J_x = \int \frac{f_e}{\gamma_e} p_{x,e} dp_{x,e}, \quad \mathbf{J}_\perp = \frac{e^2 \mathbf{A}_\perp}{m_e} \int \frac{f_e}{\gamma_e} p_{x,e} dp_{x,e} \quad (8)$$

and the fact that the transverse component of the electric field obeys $\mathbf{E}_\perp = -\partial \mathbf{A}_\perp / \partial t$. Its longitudinal part is indeed purely electrostatic, $E_x = -\partial \phi / \partial x$, with $\phi(x)$ expressing the electrostatic potential. We finally remark that in this integration scheme the longitudinal electric field is obtained through Ampere's equation (i.e. $\partial E_x / \partial t = -J_x$), which is integrated in place of Poisson's equation ($\partial E_x / \partial x = e(n_e - n_i)$) because of algorithmic convenience: to compute the longitudinal electric field at $t_n + \Delta t/2$ with Poisson's equation, the value of f at the same time would be necessary, but it is unknown. The solution to the second order accuracy of Ampere's equation is instead $E_x(x, t_n + \Delta t/2) = E_x(x, t_n - \Delta t/2) - \Delta t J_x(x, t_n)$.

4. Generation of an electron density cavitation by SIT effect

We now show some results of a simulation run of a laser–plasma interaction described by the equations introduced in Section 3, in which the SIT effect takes place. It is found that an electron cavitation arises because of Coulomb explosion on scales of the pump wavelength λ_0 .

The following parameters characterizing the plasma have been chosen: $n_0/n_c = 1.6$, $I \lambda_0^2 \simeq 5.45 \times 10^{18} \text{ W cm}^{-2} \mu\text{m}^2$ (I being the laser-light intensity), and $T_e = 100 \text{ keV}$, $T_i = 20 \text{ keV}$ (electron and ion temperature, respectively). Results similar to the ones presented in the text that follows have been found also at lower electron temperature, $T_e = 3 \text{ keV}$. The laser incident wavelength is such that $k_0 d_e \simeq 0.586$, and the pump frequency is $\omega_0 = 0.79 \omega_{p_e}$. The geometry of the system consists of a plasma slab of length $L_{\text{plas}} = 130 d_e$ (which is approximately equal to $12 \lambda_0$), surrounded by a vacuum region of $L_{\text{vac}} = 160 d_e$. The total number of grid-points is $N_x = 12800$ in space and $N_{p_x} = 512$ in both p_e and p_i momentum space. Since we have $\langle \gamma^{-1} \rangle \simeq 0.28$, the dispersion relation of electromagnetic waves inside this plasma reads: $\omega_0 = (\omega_{p_e}^2 \langle \gamma^{-1} \rangle + k_0^2 c^2)^{1/2} = 0.789 \omega_{p_e}$.

In Fig. 1 (top) the behavior of the electron distribution function is shown at the beginning of the interaction, as vortices form due to the beat-wave effect between the pump light and the wave reflected by the overdense region. Because of the SIT effect, the pump wave-front of the light penetrating in the overdense plasma represents a discontinuity in the plasma refractive index, and so acts as a relativistically moving mirror for the incident light. This causes a Doppler-shift in the frequency of the wave reflected by the discontinuity associated with the wave-front (see Ref. [8]). The penetration of the pump wave gives rise to a three-wave parametric instability, with the matching conditions $\omega_0 = \omega_r + \omega_e$ and $k_0 = -k_r + k_e$ (subscripts 0, r and e respectively refer to the incident laser light, to the reflected and to the excited electron wave). For the reflected wave $\omega_r = (\omega_{p_e}^2 \langle \gamma^{-1} \rangle + k_r^2 c^2)^{1/2}$. With our numerical parameters: $\omega_r = 0.675 \omega_{p_e}$, $\omega_e = 0.115 \omega_{p_e}$, $k_r d_e = 0.42$, $k_e d_e = 1.006$. These numerical values are in good agreement with those provided by analytical calculation, which are $\omega_r = 0.675 \omega_{p_e}$ and $k_r d_e = 0.42$. The low-frequency acoustic-like electron wave is responsible of the plasma coherent “heating” through the generation of vortical trapping structures; it obeys $\omega_e / \omega_{p_e} = (k_e d_e) (v_F / c) = 1.006 \times 0.115 \simeq 0.12$, where v_F is the wave-front velocity. The velocity of propagation of the wave-front influences the rate of generation of new vortices, created by the beat-wave process between the incident and the reflected light waves. The plasma gets progressively more turbulent, and at $t \omega_{p_e} = 1114$ the beat-wave process seems to disappear, so as the progression of the vortices (Fig. 1, center). Correspondingly, the growth of a peak in electron density located near $x = 260 d_e$ is observed, together with the creation of an intense electric field (both these features are not shown here). The pump-wave's propagation stops because of the strong increase of ion's (and electron's) density near the wave-front, which reaches peaks

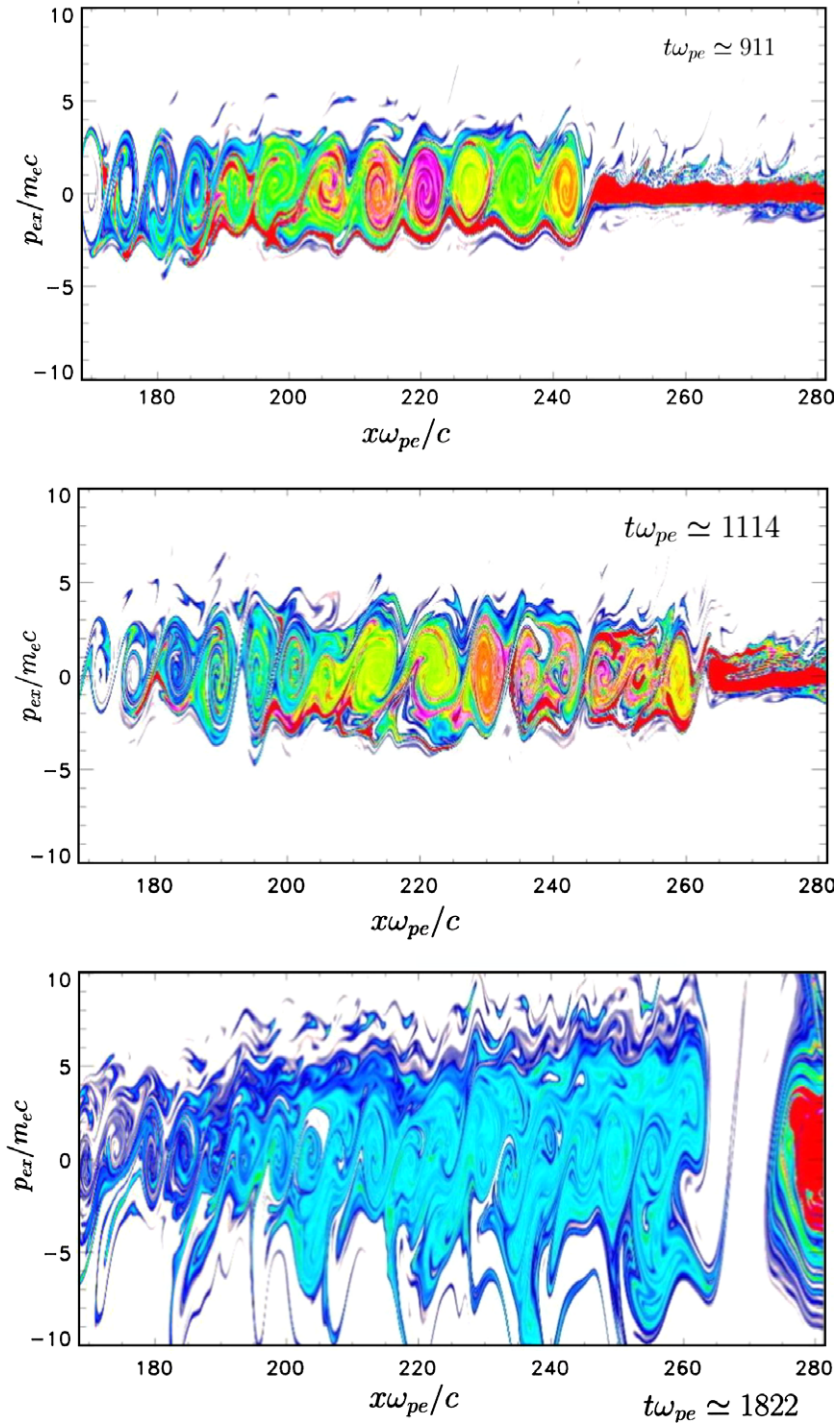


Fig. 1. Patterns of the electron distribution function inside the plasma slab, taken at different times ($t\omega_{pe} = 911, 1114, 1822$). The laser beam enters from the left along the x -axis; spatial distances are measured in d_e units. The colour-panel follows the standard colour spectrum ranging from maximum value of density (red) to minimum value (blue). The colour representation has to be taken as a qualitative indication of the relative density, since due to the ongoing wave-breaking process the reference peak-value of density is different in the three figures. E.g., the relative electron density peak (in red) just right to the density well grows from $n/n_c \approx 1.3$ (at $t = 1114$) to $n/n_c \approx 1.5$ (at $t = 1822$). (For interpretation of the references to colour in this figure legend, the reader is referred to the web version of this article.)

up to $1.8n_c$, thus making the plasma overdense for the incident laser light. An electron density cavitation is then formed (at $x \simeq 270d_e$) due to a Coulomb explosion occurring on the λ_0 scale length, and its growth destroys the vortices (Fig. 1, bottom). The plasma slab is then cut in two distinct regions: on the left side of such electron cavity the plasma keeps underdense for the pump wave, whereas on the right it does not. Because of this, hot particles are forbidden to cross from the left into the right domain, and the resulting return current is responsible of a second step of the plasma heating in this region.

5. Conclusions

In this paper, we have recalled the algorithm and computational features of a 1D–1V semi-Lagrangian Vlasov–Maxwell scheme (Section 2), and we have shown an application of it to the interaction of a strong electromagnetic wave with a moderately overdense plasma slab, in 1D-spatial geometry and in case of normal incidence, in condition suitable for the laser light propagation inside the plasma by SIT effect (Section 3). A resonant three-wave parametric instability develops between the incident pump and the Doppler-shifted reflected wave and generates an electron acoustic-like (low-frequency) mode. The plasma is then “heated” in a coherent way by the generation of trapping structures (vortices). A second stage of the process is achieved when electron cavitation arises; it induces a second turbulent electron heating because of a return current, which compensates the impediment of hot electrons to pass from the underdense to the overdense region by crossing the density cavitation (Section 4). In a forthcoming paper (Ref. [6]) it will be presented a more detailed study, performed over a wider range of values of plasma density, of the physics of the SIT wave penetration and of the related phenomena of cavitation.

We finally remark that a phenomenon analogous to the one here discussed has been recently observed in Ref. [9], in PIC simulations of the Stimulated Brillouin Scattering (SBS) in an underdense plasma. In that case, an electron cavity formation has been observed in the asymptotic regime on the time scales at which the initially cold electron population separates from ions’ dynamics; solitons trapped inside those cavities have been indicated as a possible saturation scenario of the SBS. A more detailed discussion of the kinetic features of this cavity-formation and soliton-trapping process and its possible connections to the SBS saturation must be investigated. The numerical problem addressed here (and in Ref. [7]) is one of the type for which the arguments based on the compromise between phase-space resolution and computational cost suggested in Ref. [10], would indicate a slight preferability for PIC codes (in particular for ions’ treatment) because of the dimensionality of the phase space (a $N_{\text{Vlas}}/N_{\text{PIC}} \sim 1\text{--}10$ would be obtained). Some more accurate comparisons between the two computational modelling may then be useful as a possible discriminating test for the presumed higher reliability of the Vlasov numerical approach in some kinetic regimes.

Acknowledgements

The authors acknowledge the IDRIS center (France) for computer allocation on their supercomputers. The authors are grateful to the members of the CALVI project (INRIA-Lorraine) for useful discussions.

References

- [1] Tabak M et al. *Phys Plasmas* 1994;1:1626.
- [2] Sonnendrücker E et al. *J Comp Phys* 1999;149:201.
- [3] Huot F et al. *J Comp Phys* 2003;185:512.
- [4] Cheng CZ et al. *J Comp Phys* 1976;22:330.
- [5] Staniforth A et al. *Mon Weather Rev* 1991;119.
- [6] Ghizzo A et al. *Phys Plasmas* 2007;14:062702.
- [7] Ghizzo A et al. *J Phys IV, France* 2006;133:347.
- [8] Guérin S et al. *Phys Plasmas* 1996;3:2693.
- [9] Weber S et al. *Phys Plasmas* 2005;12:43101.
- [10] Bertrand P et al. *Trans Theory Stat Phys* 2005;34:1.